


Speed Inversion in a Potts Glass Model of Cortical Dynamics

Kwang Il Ryom^{✉*} and Alessandro Treves^{✉†}

SISSA, Cognitive Neuroscience, via Bonomea 265, 34136 Trieste, Italy

 (Received 6 April 2023; accepted 11 July 2023; published 27 July 2023)

To better understand the conditions prevailing when acquiring complex, compositional memories, we introduce, in a previously studied Potts model of long-range cortical interactions, a differentiation between a frontal and a posterior subnetwork. “Frontal” units, representing patches of anterior cortex, are endowed with a higher number S of local attractor states, in keeping with the larger number of local synaptic contacts of neurons there, than in some posterior, e.g., occipital, cortices. A thermodynamic analysis and computer simulations confirm that disorder leads to glassy properties and slow dynamics but, surprisingly, the frontal network, which would be slower if isolated, becomes faster than the posterior network when interacting with it. From an abstract, drastically simplified model we take some steps towards approaching a neurally plausible one, and find that the speed inversion effect is basically preserved. We argue that this effect may facilitate learning, through the acquisition of new dynamical attractors.

DOI: [10.1103/PRXLife.1.013005](https://doi.org/10.1103/PRXLife.1.013005)

I. DO LOCAL ATTRACTORS OBSTRUCT CORTICAL DYNAMICS?

For the brain to store new memories, neural dynamics should accurately reflect the novel information to be encoded; whereas to utilize previously stored memories, the information they contain should be reliably recovered, irrespective of what is currently occurring outside. In a massively recurrent neural system, reliable retrieval has been associated with previously established *attractors* of the dynamics: as neural activity rapidly approaches its attractors, the role of afferent inputs is minimized, essentially reduced to setting the initial conditions, which select among the attractors [1]. When acquiring new memories, instead, the corresponding attractors do not exist yet. How can the existing, unrelated attractors be prevented from taking over also when they should not, and swamp the fresh information conveyed by the inputs? In physics terms, unrelated attractors amount to quenched noise, and input information has to navigate the dire straits between quenched and fast noise—rapid variability. In the mammalian hippocampus, it appears that evolution has addressed this version of the *stability-plasticity dilemma* [2] by introducing, before the massively recurrent CA3 network (the core component of hippocampal circuitry), a dedicated preprocessor, the dentate gyrus (another component), to counter any takeover by CA3 attractors [3]. In the cortex, however, there is no dentate gyrus, but also the dilemma plays out differently because of the multilevel structure. Locally, in a small portion of cortex, attractor dynamics *is* expected to dominate most of the time,

also when acquiring new memories, insofar as these are new combinations of elements, which individually have already been assigned a stable neural representation. Thus, most viewers of the 2022 FIFA World Cup final would have had already established neural representations of a soccer ball, of the scene of a penalty kick, probably of French player Mbappé as well, but would still have to form memories of the (multiple) novel combinations of these elements which occurred then. Imagine a viewer’s brain as Mbappé is about to kick the ball. Can cortical activity follow the incoming inputs, and flow freely around preexisting combinations of these elements, like a stream unimpeded by the pebbles and cobbles on its bed?

It can, to the extent that global cortical dynamics are fluid rather than *glassy*, a critical issue which in this context has received limited or no attention. Glassy behavior might in fact be made even more rigid by local attractors, widely hypothesized to serve as the ubiquitous mechanism for expressing memory functionality at the level of a small portion of cortex [1,4]. Local attractors amount to nonlinearities, which can be expected to obstruct the continuous flow of neural activation, and slow it down, adding to the quenched noise, including that due to preexisting combinations of elements. Higher levels of rapid variability—fast noise—would counter these effects, but further decrease the fidelity to the afferent inputs, i.e., the accuracy of the neural code.

Global oscillations in cortical state, as well as electroencephalographic and magnetoencephalographic response patterns, have been approached with linear decomposition analyses, such as spherical harmonics [5–7]. Yet, these macroscopic descriptions gloss over precisely local attractor dynamics, the key factor that may impede global dynamics.

The compartment model by Braitenberg [8] offers a conceptual framework to remedy such neglect. It proposes a separation between local and long-range cortical interactions, both of which are envisaged to express associative plasticity and thus to contribute to associative memory. The Potts associative network [9] can then be construed as an effective

*kryom@sissa.it

†ale@sissa.it

model of long-range interactions, that subsumes local ones into the *ad hoc* dynamics of Potts units, with S states each, which represent patches of cortex [10]. The S states, pointing in S different directions, model the local attractors of a patch of cortex, and they may be dynamical rather than pointlike attractors [11]. We have analyzed the spontaneous *latching* dynamics induced by adaptation and inhibition [12] and discussed how they could play out in free recall paradigms [13]. Here, we focus instead on input-driven dynamics, and whether they are fluid or glassy.

II. A DIFFERENTIATED POTTS MODEL

Previous studies had reduced the cortex to a *homogeneous* network of Potts units, each of which is characterized by the same number of states, S , positive feedback w , time constants τ for excitation, inhibition, and adaptation. This is in contrast with prominent features of cortical organization, which, for example, point at much higher numbers of local synaptic contacts among pyramidal cells in temporal and frontal, compared to occipital, cortex [14], suggestive of a capacity for more and/or stronger local attractor states in the former, or conversely at more linear and prompt responses to afferent inputs in posterior visual cortices [15,16], suggestive of reduced positive feedback relative to more anterior areas. Other features show gradients that roughly align with these, and all together have been proposed by Changeux and colleagues [17] to define, in particular in the human brain, a *natural cortical axis*. If one attempts to incorporate these features into a *nonhomogeneous* Potts network, what are the implications for cortical dynamics? The indications that the dynamics in frontal cortex may be more affected by local attractors need not necessarily imply, it should be noted, that individual neurons are routinely “stuck” in steady states, in which they keep firing at steady rates for a few hundred milliseconds. This would be in apparent contrast with extensive evidence for more dynamical forms of coding in frontal cortex, e.g., for changing task contingencies rather than stable visual features [18]; or, moving up to entire populations of neurons and to the human brain, for the encoding of verbs rather than nouns [19,20] (but see Ref. [21]) or of syntax rather than the lexicon [22]. As noted above, stable local attractors may be expressed by rapidly changing firing rate distributions [11] and also quasistable attractor “ruins” may in fact accelerate dynamics when particularly strong [23].

Local attractor states may thus be composed, only transiently or more persistently, into global attractor states. Studying the dynamics of reactivating such global attractors requires assumptions about the nature and the statistics of the compositionality, and we have analyzed two distinct models in this respect, both for a homogeneous Potts network [24,25]. Here, however, we want to focus on the dynamics unfolding away from previously acquired global attractors, as new attractors are being established, or *learned*. In a learning regime, we expect the lack of *a priori* relations between what has been already acquired and the new compositional representation to be established to turn the cortex, from the point of view of the latter, into basically a disordered system. Do long-range cortical interactions then result in “glassy” dynamics, with critical slowing down and persistent traces of initial condi-

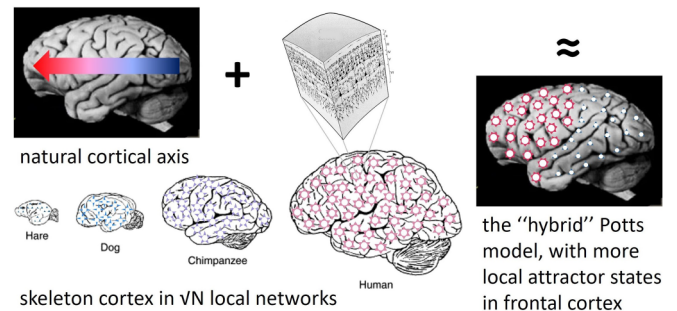


FIG. 1. The hybrid Potts model combines the representation of local attractor dynamics in terms of units with S active states, inspired by Braitenberg’s idea of an approximate \sqrt{N} scaling [8], with a differentiation between frontal and posterior cortices, along the natural axis posited by Changeux and others [17] and expressed by a larger S value for frontal units. Note the assumption that the critical quantity that varies along the axis is S , the simplification of replacing a gradient with just two S values, and the ill-fitting temporal cortex areas, in which pyramidal cells have abundant recurrent collaterals [14] but are otherwise included among posterior regions.

tions? During learning, that would likely imply an inability to track new inputs. If so, how does the glassy character express itself over the short timescales relevant to cognition? Is it affected by gross inhomogeneities, like the posterior-anterior gradients in cortical parameters mentioned above?

We are aware of the large distance between our abstract models and the real cortex, but we choose to consider here the most basic and mathematically well-defined aspects of these issues, by analyzing a *hybrid* model that integrates in the Potts formulation a crude binary version of the gradient along the “natural” axis (Fig. 1), and leave for later reports more realistic models of cortical dynamics and applications to other domains. As we will see, even the analysis of what seems like a simple extension of a standard model for an infinite-range spin glass reveals some surprising properties.

III. MEAN-FIELD ANALYSIS OF THE LONG-TIME BEHAVIOR

As discussed in previous reports [26,27], the analysis of the attractor states of associative Potts networks, in which each unit represents a patch of cortex, relies on the same assumption of symmetric interactions, proposed for the standard model [28] in which each unit represents a single neuron. We aim to sketch in this section the thermodynamics of the simplest version of the model, and then of the variant divided into two subnetworks, which differ in the number S of states per unit.

If we consider, as we do here, a local cortical network to behave effectively as a *discrete* Potts unit, $\sigma_i \in \{0, 1, \dots, S\}$, which can take one of S active states (labeled by $k = 1, 2, \dots, S$) as well as stay in the quiescent state (labeled by 0), it is convenient to define the model in terms of the Potts spin operator,

$$V_i^k \equiv (\delta_{\sigma_i, k} - 1/S)(1 - \delta_{\sigma_i, 0}). \quad (1)$$

A. The random homogeneous Potts model, with a zero state

First, we consider a network of Potts units all endowed with the same number of states, S , that interact through random tensor connections. The Hamiltonian of the system reads

$$H = -\frac{1}{2} \sum_{i \neq j} \sum_{k, l > 0} J_{ij}^{kl} V_i^k V_j^l + U \sum_i (1 - \delta_{\sigma_i, 0}), \quad (2)$$

where N is the number of Potts units, U is a threshold [12], and the $\{J_{ij}^{kl}\}$'s are sampled from Gaussian distributions with mean J_0/N and variance $\lambda^4 J^2/N$. We have introduced the normalization factor λ ,

$$\lambda^2 \equiv \frac{S}{\sqrt{S-1}}, \quad (3)$$

which makes the critical temperature for the transition to a glassy phase independent of S , in units of J (see below). The interactions satisfy

$$\begin{aligned} J_{ji}^{kl} &= J_{ij}^{lk}, \quad i \neq j, \\ J_{ii}^{kl} &= 0. \end{aligned} \quad (4)$$

Note that in this model, although S is the same across all units, the states of one unit do not correspond to those of another unit, as they would if they represented, e.g., directions in physical space. This is in contrast to the Potts model considered by Elderfield and Sherrington (ES) [29], in which such correspondence holds, and the interactions, albeit still random, are in the form $J_{ij}^{kl} \propto J_{ij}(\delta_{kl} - 1/S)$, with a single random variable J_{ij} per unit pair (and, in addition, there is no quiescent state). In that model, the symmetry among Potts states is global, whereas in our model it is local, as it must be in order to represent distinct codes by different patches of cortex.

Despite the larger number of random variables, the thermodynamic analysis proceeds along similar lines to that in Ref. [29] and it is in some respects simpler. Using the replica method [30], the free energy of the system is written as reported in Appendix A.

Properties near the critical temperature

The paramagnetic solution ($q_{\gamma\delta} = 0$, $\gamma \neq \delta$) is the ground state of the system at high enough temperatures. Lowering the temperature, a phase transition from the paramagnetic to the spin glass phase occurs at $T = T_c$. To determine T_c , one can (Landau-)expand the free energy close to it, as shown in Appendix B. Defining suitable coefficients A , B , C , and D and $\psi \equiv 2q_{\gamma\gamma}/(S-1)$ in terms of the order parameter $q_{\gamma\gamma}$ (assumed not to depend on the replica index γ near T_c), ψ should satisfy

$$\psi = \frac{\exp[(\beta J)^2 \frac{S(S-1)}{2} \psi - \beta U]}{1 + S \exp[(\beta J)^2 \frac{S(S-1)}{2} \psi - \beta U]} \quad (5)$$

and the quantity $S\psi$ gives the fraction of active units in the network.

Under the replica symmetric (RS) assumption, $q_{\gamma\delta} = q$ ($\gamma \neq \delta$), the critical temperature is determined by numerically solving

$$(\beta J)^2 S^2 \psi^2 - 1 = 0 \quad (6)$$

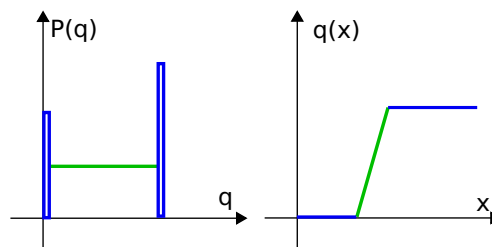


FIG. 2. Schematic description of replica symmetry breaking, from Eq. (9). Left: The probability density $P(q)$, with blue rectangles denoting Dirac delta functions. Right: Parisi's function. Color coding is used to facilitate a visual comparison.

together with Eq. (5), since ψ contains T . If $U \rightarrow -\infty$ (which amounts to considering the case with no quiescent state; all units are active if the threshold is infinitely low), then $S\psi \rightarrow 1$ and we get a simple formula, $T_c = J$, or $T_c = 1$ in units of J . The phase transition is a continuous one if

$$0 < 4S\psi - (S-2). \quad (7)$$

For $S < 6$, there exists a critical value of U , U_c , above (below) which the transition is discontinuous (continuous). For $S > 6$, the transition is discontinuous for all values of U .

A discontinuous transition is indicative of more pronounced glassy effects for larger S , suggesting that cortical networks with a larger number of local attractors may be slower. This RS solution is, however, unstable against replica symmetry breaking (RSB) in the whole glassy phase. Thus, the question should be reexamined after breaking replica symmetry in the analytical approach.

To probe replica symmetry breaking, following Parisi's hierarchical scheme [31] we write the free energy

$$\begin{aligned} -\beta f \approx & \int_0^1 dx \left[\frac{A}{2} q^2(x) - \frac{B}{3} q^3(x) - \frac{D}{12} q^4(x) \right] \\ & + \frac{C}{3} \int_0^1 dx \left[x q^3(x) + 3q(x) \int_0^x q^2(y) dy \right], \end{aligned} \quad (8)$$

using the coefficients A , B , C , and D defined in Appendix B, and this free energy is to be maximized with respect to Parisi's function $q(x)$ [32]. We note that Eq. (8) has the same form as in the ES model [29], except for the coefficients. Thus, we can envisage that the nature of RSB is similar to that in the ES model (see also Refs. [33,34] for its detailed properties). The nontrivial solution to the maximization of the free energy in Eq. (8) is

$$q(x) = \begin{cases} 0, & x \leq x_0 \\ \frac{Cx-B}{D}, & x_0 \leq x \leq x_1 \\ q_1 = \frac{A}{B-C} + O(q_1^2), & x_1 \leq x, \end{cases} \quad (9)$$

where

$$x_0 = \frac{B}{C} = \frac{1}{2\psi} \frac{S-2}{S}, \quad x_1 = \frac{B}{C} + \frac{AD}{C(B-C)}. \quad (10)$$

From Eq. (9), we can see how replica symmetry is broken, for a given value of U . The scheme in Fig. 2 is similar to the one for the ES model. Note that x_0 is always zero for $S = 2$, regardless of U , whereas it remains positive for $S > 2$.

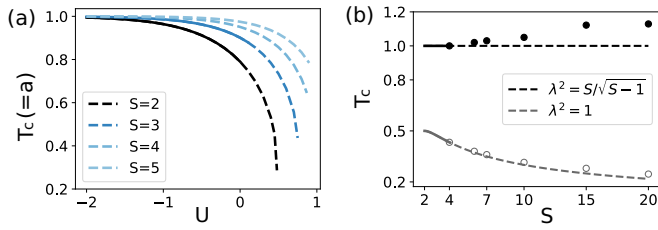


FIG. 3. The critical temperature (T_c) for the onset of the glassy phase of a homogeneous Potts network. (a) T_c as a function of the threshold U for a model with a zero state. With the normalization set as in Eq. (3), the mean activity a of the network at $T = T_c$ is equal to T_c itself (that is, to T_c/J). Dashed curves are predicted by RS theory and solid curves are from RSB theory. All transitions shown here are continuous. (b) T_c as a function of S for a model without a zero state ($U \rightarrow -\infty$): color encodes the normalization used (as indicated in the legend). Solid curves are obtained analytically from the Landau expansion of the free energy (a continuous phase transition) and dashed curves are their mere extensions, to guide the eye. Circles are obtained by numerically maximizing the one-step RSB free energy (a discontinuous transition), Eq. (B7). We set $J = 1$.

This means that $P(q)$ has a Dirac delta at $q = 0$ for $S > 2$, whereas there is no Dirac delta at $q = 0$ for $S = 2$, as in the Sherrington-Kirkpatrick (SK) model. The phase transition to the glassy phase is continuous if

$$\begin{aligned} 0 < 2S\psi - (S - 2), \\ 0 < 3S^2(3S - 1)\psi^2 - 12S(S - 1)\psi + S^2 - 3S + 3. \end{aligned} \quad (11)$$

In general, these two conditions are numerically probed together with Eqs. (5) and (6) for a given value of U . As a special case, when $U \rightarrow -\infty$, the second condition is guaranteed. However, unlike RS Eq. (7), the first of RSB Eqs. (11) ceases to hold for $S > 4$. Thus, the transition can be continuous only for $S \leq 4$. We can compute the range of U where Eqs. (11) hold by solving them together with Eq. (5) and Eq. (6). The result is shown in Fig. 3(a).

Thus, in practice, replica symmetry breaking has lowered the value S beyond which the transition to the spin glass phase must be discontinuous from $S = 6$ to $S = 4$, while still suggesting that, in general, cortical networks with a larger number of local attractors may be slower.

What happens, if the transition is discontinuous, in the entire range $0 < T < T_c$? In general for spin glasses the analysis via the replica method is complicated and involves heavy numerics; however, for Potts spins specific circumstances enable an approach, explained in Appendix B, that allows to extract at least an estimate of T_c itself, as reported in Fig. 3(b).

In conclusion, the level of fast noise below which the Potts network is glassy, T_c , is with the λ normalization we adopt [Eq. (3)] roughly independent of the number of states, S , its units are endowed with; but the way it enters the glassy phase depends markedly on S , and it appears that with larger S the entrance is more abrupt, suggestive of more impeded glassy dynamics.

B. The hybrid Potts model without a zero state

We now consider a network of Potts units that have different values for S : a unit i has its own number S_i of Potts states.

For the sake of simplicity, we consider Potts units without the quiet state (equivalent to taking the limit $U \rightarrow -\infty$). We group units according to their number of states: there are N_l units in group l ($l = 1, 2, \dots, L$) and they have S_l Potts states each. If the total number of Potts units in the network is N ,

$$\eta_l \equiv \frac{N_l}{N}, \quad 1 = \sum_{l=1}^L \eta_l.$$

We write

$$H = -\frac{1}{2} \sum_{i \neq j} \sum_{k=1}^{S_i} \sum_{m=1}^{S_j} \lambda_i J_{ij}^{km} \lambda_j (\delta_{\sigma_{ik}} - 1/S_i) (\delta_{\sigma_{jm}} - 1/S_j), \quad (12)$$

where $\lambda_j \equiv \sqrt{(S_j/\sqrt{S_j-1})}$ normalizes the interactions with both a pre- and a postsynaptic factor, and the $\{J_{ij}^{km}\}$'s are sampled from a Gaussian distribution of mean J_0/N and variance J^2/N and satisfy Eqs. (4).

The replica method proceeds as detailed in Appendix B.

The critical temperature for the onset of the glassy phase is again given by

$$T_c = J, \quad (13)$$

where the phase transition is continuous in terms of q whenever

$$\sum_{l=1}^L \eta_l \frac{S_l - 4}{\sqrt{S_l - 1}} < 0. \quad (14)$$

As an example, consider a hybrid network with two types of Potts units: half with S_1 and half with S_2 states. The phase transition is continuous if

$$\frac{S_1 - 4}{\sqrt{S_1 - 1}} + \frac{S_2 - 4}{\sqrt{S_2 - 1}} \leq 0. \quad (15)$$

Several cases are interesting (we set $1 < S_1 \leq S_2$):

- (i) $S_1 = 2$. The transition is continuous for $S_2 \leq 10$ and discontinuous otherwise.
- (ii) $S_1 = 3$. The transition is continuous for $S_2 \lesssim 5.5$ and discontinuous otherwise.
- (iii) $S_1 \geq 4$. The transition is always discontinuous (except for $S_1 = S_2 = 4$, but then the network is again homogeneous, as in the previous section).

C. The glassy phase of a Potts associative memory

We consider now an attractor neural network comprised of Potts units. The Hamiltonian is the same as in Eq. (2), with the connection J_{ij}^{kl} now given by the Hebbian learning rule,

$$J_{ij}^{kl} = \frac{1 - \delta_{ij}}{Na(1 - \bar{a})} \sum_{\mu=1}^p (\delta_{\xi_i^\mu k} - \bar{a})(\delta_{\xi_j^\mu l} - \bar{a})(1 - \delta_{k0})(1 - \delta_{l0}), \quad (16)$$

where $\{\xi_i^\mu\}$ are p randomly correlated memory patterns, a is their sparsity, and $\bar{a} = a/S$. The free energy and the saddle-point equations are obtained by the replica trick, as sketched in Appendix C. One can solve them by using either RS or RSB assumptions to compute, *inter alia*, the storage capacity of the network. We refer to Refs. [26,27] for a discussion of the storage capacity (see also Refs. [9,35] for related but different

models). Here, we are interested in the phases prevailing at higher temperature, where there are no retrieval solutions: the paramagnetic phase and the glassy phase.

A phase transition from the paramagnetic to the glassy phase occurs at

$$T_c = \tilde{q}\tilde{a} + \psi\tilde{a}\sqrt{\alpha(S-1)} \rightarrow \frac{(S-1)a}{S^2} + \frac{a}{S^2}\sqrt{\alpha(S-1)}, \quad (17)$$

where $\alpha = p/N$ and the last expression is for the limit of $U \rightarrow -\infty$ (i.e., in the absence of a quiet state). It is a continuous transition if $S \leq 6$. For $S > 6$, the transition is continuous if $\alpha < \alpha_0$ and discontinuous otherwise, with

$$\alpha_0 = \frac{16S^2\psi^2(S-1)}{(S-4\psi S-2)^2} \rightarrow \frac{16(S-1)}{(S-6)^2},$$

where the last expression is again for $U \rightarrow -\infty$.

As in the random Potts model considered above, there is a value of U above which the phase transition cannot be treated by the Landau expansion, indicating that, when lowering T , the glassy phase is entered discontinuously, with an abrupt freezing of the Potts units in a disordered configuration. This result is shown in Appendix C.

The general conclusion of these thermodynamic analyses is that a continuous transition to a glassy phase characterizes disordered networks of Potts units with low S , whereas networks with high S tend to get stuck more abruptly. Before applying these insights to, respectively, posterior and frontal cortical networks, however, we should study the actual dynamics of the Potts model.

IV. DYNAMICS

Although dynamics can be studied within mean-field theory to a certain extent [36,37], here we stick to Monte Carlo (MC) simulations. Throughout this work, we use the heat bath algorithm to simulate the dynamics of Potts networks. Specifically, the local field of each Potts unit is computed as

$$h_i^k = \sum_{j=1(j \neq i)}^N \sum_{l>0} \left(J_{ij}^{kl} - \frac{1}{S} \sum_{k'} J_{ij}^{k'l} \right) V_j^l, \quad k > 0, \quad (18)$$

where the weights J_{ij}^{kl} express the random or the associative memory model. At each MC step, one Potts unit is randomly chosen to be updated based on the following equations:

$$\begin{aligned} \text{Prob}[\sigma_i = k] &= \frac{\exp[\beta h_i^k]}{\sum_{l=1}^S \exp[\beta h_i^l] + \exp[\beta U]}, \quad k > 0, \\ \text{Prob}[\sigma_i = 0] &= \frac{\exp[\beta U]}{\sum_{l=1}^S \exp[\beta h_i^l] + \exp[\beta U]}. \end{aligned} \quad (19)$$

For models without a zero state, the second of Eqs. (19) is not used.

For most of the simulations presented here, we run two systems [38] with the same quenched disorder (i.e., the set of interactions between Potts units) and measure the overlap between the two configurations γ and δ at time t :

$$q_{\gamma\delta}(t) = \frac{S}{N(S-1)} \sum_{i=1}^N (\delta_{\sigma_i^\gamma \sigma_i^\delta} - 1/S). \quad (20)$$

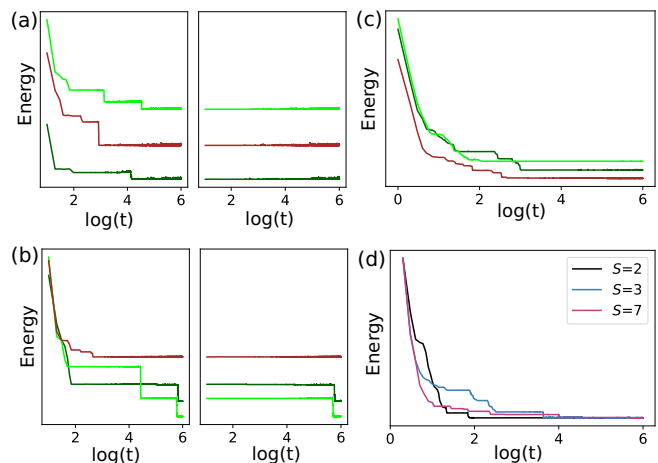


FIG. 4. Energy as a function of MC sweeps per unit for sample MC trajectories. Note the logarithmic scale of the abscissa. (a) Three example trajectories are shown for a homogeneous Potts network without a zero state and with $S = 2$. In the right-hand panels, t restarts after $t_0 \simeq 10^5$, to focus on long-time glassy dynamics. (b) Same as (a) but with $S = 7$. (c) Example trajectories of a homogeneous Potts network with a zero state ($S = 3$). (d) Example trajectories of the ES model [29]. The three curves are rescaled and shifted for better visibility [only in panel (d)]. Note that the ES model reduces to the SK model if $S = 2$. The number of units is $N = 256$ for all panels, and each data point is averaged over 10 MC sweeps, except for the first 100 points.

A. Dynamics close to steady states

Figure 4 shows sample trajectories of networks with random interactions at temperatures $T \ll T_c$, to illustrate their glassy nature: after an initial transient the system is trapped in metastable states for a while before finding a way out, along which it can further lower its energy. The opportunities to escape a metastable state, however, become rarer and rarer, and the time spent near it longer and longer, a process called thermalization.

To measure how fast the dynamics unfolds on the glassy free energy landscape, we first “thermalize” a configuration by letting it evolve for $t_0 = 10^3$ time steps, and then start from it two simulations with identical interactions, until at τ their overlap reaches half its initial value. Since the times τ are quite scattered depending on the realization of the interaction—their logarithms are approximately normally distributed—we consider their cumulative distribution, for a given network, and in particular the thermal *half-life* scale $\zeta_g(T)$, defined as the median $\mu_{1/2}[\log(\tau)]$ when the cumulative distribution, at a temperature T , reaches the value 0.5.

With this procedure, we find that a homogeneous random Potts network “moves” faster the lower is S , i.e., the number of states of its Potts units. This is shown in Fig. 5(a), which indicates that $\zeta_g(T) \equiv \mu_{1/2}[\log(\tau)]$ increases approximately with $\log(S)$, with the parameters we use. This is in line with the expectations from the thermodynamic analysis.

If we measure τ (and ζ_g) separately for the units with a given S in a hybrid network, we find that the small- S units get slower and the large- S units get faster, due to the hybridization. Surprisingly, however, the effect is not simply

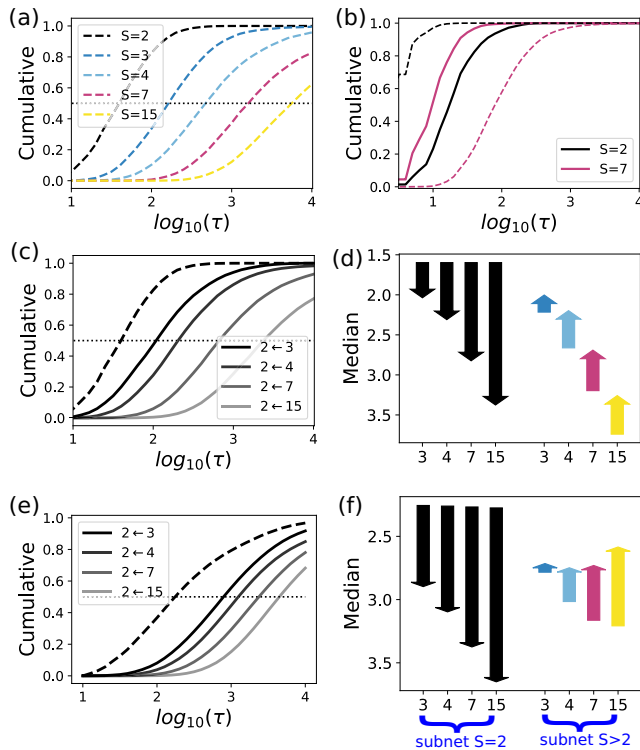


FIG. 5. Speedup and slowdown in a hybrid Potts model. All curves are dashed for homogeneous nets, solid for hybrid ones. (a) Cumulative distribution of τ , computed for homogeneous networks of $N = 256$ units, as a function of S . (b) The inversion of speed due to hybridization between small units with $S_1 = 2$ and large units with $S_2 = 7$. Note the faster dynamics, as we have set here $T = 0.8$, whereas the default value $T = 0.5$ was used in the other panels. (c) A subnetwork of $S_1 = 2$ that interacts with another subnetwork with $S_2 > 2$, denoted in the legend as $2 \leftarrow S_2$, is more slowed down the higher is S_2 . Note that the case with $S_2 = 2$ is the homogeneous network of panel (a). (d) The speedup and slowdown of the subnetworks in panel (c) are shown by the arrows, which head up for units that accelerate. The color of bars stands for S as in panel (a), while the height measures the difference $\Delta\zeta_g$ in the median of the cumulative distribution of $\log(\tau)$, between hybrid and homogeneous networks. Start and end points of arrows are the median $\zeta_g(T)$ for homogeneous and hybrid network. [(e), (f)] Same as (c) and (d), but without the normalization constants λ_i in Eq. (12) and $T = 0.2$, $t_0 = 5 \times 10^3$.

an interpolation or averaging of the temporal scale between the two subnetworks, that would come to share a common speed, because in many cases the large units get markedly faster than the small units. This is shown in Fig. 5(b) for $T = 0.8$ and large units with $S_2 = 7$, that interact in a hybrid network with small spins, $S_1 = 2$. Figure 5(c) shows that the slowing down of these spins scales roughly with the logarithm of S_2 , the number of states of the units that “bog them down.” Simultaneously, the large units “speed up” after the hybridization [Fig. 5(d)] and, particularly when the interactions are not renormalized as in Eq. (12), can get to be faster, on average, than the small spins [Fig. 5(f)].

The speed inversion phenomenon indicates that the same free-energy landscape is “perceived” as rougher, near the metastable states, by Potts units with fewer degrees of

freedom. Notably, the effect occurs, albeit reduced in size, with the normalization of Eq. (12), which according to the thermodynamic analysis makes the relevant fast noise range $0 < T < T_c$ independent of S . Does the same effect occur away from the metastable states, e.g., in the initially rapid dynamics to the left of the panels in Fig. 4, or when *asymmetric* connections weaken the very stability of such disordered states?

B. Factors that accelerate the dynamics

In the Hopfield model, imposing symmetry in the interactions, which established the connection with Hamiltonian systems, thus enabling the analytical approach [28], entailed gross disregard for Dale’s law—stating that excitatory and inhibitory neurotransmitters are released by distinct types of cortical neurons—and also of plausible statistical models of connectivity among excitatory neurons alone. Interestingly, it was argued early on that spin-glass-like metastability would still characterize networks with asymmetrically “diluted” connectivity, whereas it was suggested that more profound changes due to asymmetry might be observed in the dynamics [39]. In the Potts network, inspired by Braitenberg’s model [8], Dale’s law is not relevant as long-range connectivity (the component modeled by the tensor interactions among Potts units) is only excitatory; there is no urgency to consider diluted connectivity either, as the tensor connections themselves are considered to recapitulate thousands of individual synaptic connections [27]. Still, it makes sense to consider the effect of asymmetric nonzero values in the random interactions, by writing them in the form

$$J_{ij}^{kl} = \gamma J_{\text{asym}} + (1 - \gamma) J_{\text{sym}}, \quad (21)$$

where $J_{ij,\text{sym}}^{kl} = J_{ji,\text{sym}}^{lk}$ and $J_{ij,\text{asym}}^{kl}$ is unrelated to $J_{ji,\text{asym}}^{lk}$; thus the former are *symmetric* and the latter *asymmetric* random components, drawn from the usual distribution with zero mean and variance J .

Figures 6(b) and 6(c) show that introducing asymmetry does have a major effect in speeding up the dynamics, across the board, while maintaining the slowing down of small units and speeding up of large units due to hybridization. With $\gamma = 0.3$, the root-mean-square symmetric component of the weights is still more than twice the asymmetric component, and yet dynamics are extremely fast.

To probe the dynamics away from the vicinity of the metastable states, without touching the symmetry of the interactions, we use a variant of the simulation paradigm above, that mimics the arrival of an external input to the Potts network. That is, after a configuration has been thermalized as in previous simulations, a fraction of the units are randomly reset in a new state (different from the thermalized one), and then two independent trajectories evolve with the heat bath procedure from this common starting configuration, until the time τ when their overlap has been halved. Figure 6 shows that the basic inversion effect, and in particular the selective slowing down of the “small” units, persists over wider regions of activity space. With respect to the standard thermalization paradigm in Fig. 6(a), Fig. 6(d) shows that resetting a quarter of the units does indeed accelerate the dynamics of the $S = 3$ network, when it is homogeneous, whereas when it is

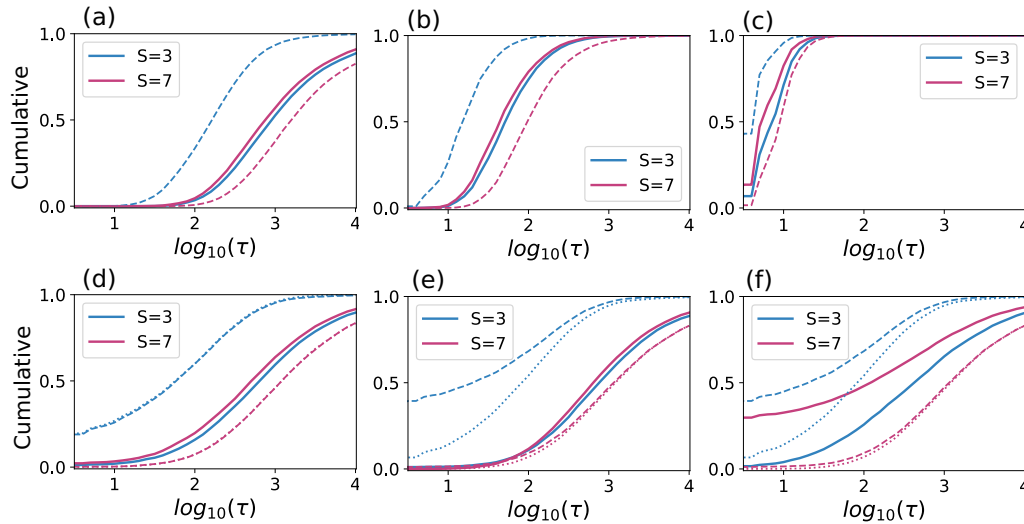


FIG. 6. Speeding up the dynamics with asymmetric connections and external inputs. (a) The speedup and slowdown of subnetworks (relative to their homogeneous counterparts) are shown without asymmetry or perturbation, to serve as the “control” case. (b) The effect of asymmetry, where $\gamma = 0.2$, is to speed up the dynamics across both subnetworks, homogeneous or hybrid. (c) With more asymmetry, $\gamma = 0.3$, the same general speedup is seen as in (b), but more extreme. (d) $N/4$ units are perturbed or reset, after thermalization, mimicking an external input; they are selected uniformly across the whole network. $\gamma = 0$. (e) Those perturbed by the input are all in the smaller unit ($S = 3$) subnetwork. (f) They are all in the larger unit ($S = 7$) subnetwork. In both (e) and (f) the dotted curves refer to unperturbed halves of homogeneous networks, and the dashed ones to the halves including the units receiving the input.

hybridized with $S = 7$ units, these latter get faster, and slightly faster than the $S = 3$ ones.

In Fig. 6(d), the external stimulus or perturbation is applied to a quarter of the units distributed in both subnetworks; when they are concentrated among the small $S = 3$ units [Fig. 6(e), solid curves], the already minimal acceleration effect is reduced even further. When they are concentrated among the large $S = 7$ units, instead, their subnetwork activity is markedly accelerated, as expected [Fig. 6(f), solid curves], but only if it is part of a hybrid network with $S = 3$ units, with only minimal acceleration if they are part of a homogeneous network.

The results of the simulated external input procedure are therefore rather counterintuitive. If affecting one-fourth of the Potts units, the input effectively distances the network from its slow-evolving glassy state in two situations: when it is applied to a homogeneous network of small but not large units, *or* in a hybrid network, only when it is applied to the large units, but then it accelerates essentially their dynamics alone. These complex effects are observed still within the domain of networks with symmetric interactions, and they beg the question of what happens when an external input is combined with relaxing the symmetry constraint in a more cortically plausible manner.

C. Approaching a cortical scenario

An interesting model of how cortical dynamics might influence cortical connectivity might be expressed by setting $\gamma = 0$ only for the interactions among the small units, to express the hypothesis that during learning they had been almost *clamped* by afferent inputs. This leads to a remarkable inversion effect, illustrated in Fig. 7(a). One can see a

self-consistent pattern potentially at play: the hybridization makes the large- S subnetwork fast, which upon *spike-timing-dependent* synaptic plasticity would tend to result in more asymmetric tensorial couplings connecting those units.

To combine a putative external sensory input and the same type of asymmetry of Fig. 7(a), in a cortically plausible scenario, we show in Fig. 7(b) what happens when resetting a fraction η of the small- S units (thus simulating an input to posterior cortex) after thermalization. The result is a moderate general speedup, for both subnetworks, and very fast dynamics in about 30% of the runs, for the posterior network. It appears that in those runs the input has brought the small- S units close to the boundary between deep basins of attraction, so that fast noise leads to the immediate divergence of trajectories with the same starting point. For most of the other runs, instead, presumably well inside each large basin, the posterior network remains slower than the frontal one.

Finally, in Fig. 7(c) we take a major step towards cortical plausibility, by reintroducing the quiet state until now considered only in the thermodynamic analysis. The quiet state implies sparse activity (only a fraction a of the Potts units in one of their active states) and this overall level of sparsity must be conceived as being regulated by inhibition (in the analysis, this amounts to considering the activity level rather than the threshold U as a parameter, whereas for the implementation in the simulations, see Appendix D). We first consider in this case purely symmetric random connections, and an input applied to some of the posterior units. To maintain the sparsity level, the input is applied after thermalization both to units already in an active state (which are then flipped to a different state) and to units in their quiescent state—in this case the input is *clamped* to keep them in the new state, simulating the strong effect of thalamic inputs impinging on an inactive local

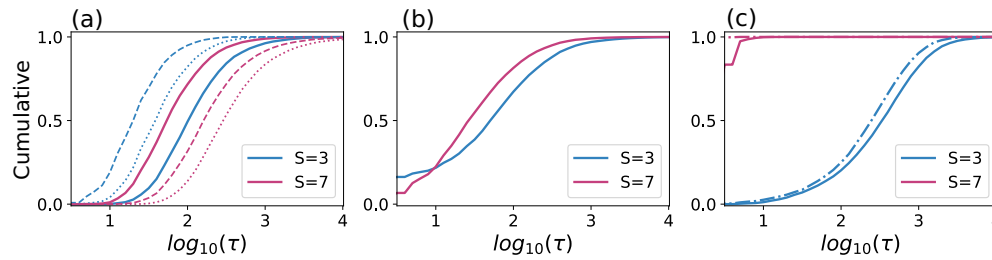


FIG. 7. The speed inversion effect likely applies to the cortex. (a) Distribution of divergence times when the asymmetric component is zero only within the $S = 3$ subnetwork and $\gamma = 0.2$ otherwise. For homogeneous networks, dotted curves are for the subnetworks that have zero asymmetric component. (b) Same as in (a), but half the $S = 3$ subnetwork units are perturbed after thermalization. (c) Potts glass model with a quiet state and with regulated mean activity. After thermalization, a persistent external input is applied to the $S = 3$ subnetwork, by flipping to a different active state a proportion $a\eta$ of its active units, inactivating a proportion $(1 - a)\eta$, and activating (in a random active state) the exact same number as those that get inactivated (which is close to $Na(1 - a)\eta$, but varies somewhat in the course of each thermalization). The newly activated units are clamped. Broken curves show results when reintroducing asymmetry, $\gamma = 0.2$, in the connections involving the $S = 7$ units.

network. Again, we refer to Appendix D for a full description of the procedure. The result, in Fig. 7(c), is a strong differentiation between slow dynamics in the posterior network and an immediate divergence of nearly all trajectories in the frontal one. While this outcome stems to a large extent from clamping a few critical units only in the posterior network, it suggests that the main speed inversion phenomenon is not necessarily reversed back again when moving towards actual cortical dynamics. Reintroducing the asymmetry in the connections involving the $S = 7$ units only makes their network diverge immediately in *all* trajectories [the broken curves in Fig. 7(c)].

D. Short-term dynamics for the associative memory model

In this last Results section we consider the associative memory model, in which the interactions are not random but rather tend to align the network along one of a number p of preacquired memory states. Here there is no hypothesis about the overarching structure of memory representations in the cortex (we have reported elsewhere on the problems in applying to the cortex the simplest autoassociative retrieval scenario [25]) but rather we aim to assess the effects on glassy dynamics of the presence of the large attractors associated

with the memories. The logic is that we are probing the establishment of new representations, driven by either external inputs or internal dynamics, and if the network gets stuck into a previously acquired memory, no new configuration can be learned.

First, Fig. 8(a) shows that hybridization, i.e., the differentiation between large- and small- S units, in this case speeds up both subnetworks. In a homogeneous network, the $S = 7$ units are extremely slow, as nearly all trajectories are trapped in one of the large basins of attraction of the memories encoded in the connections, reflecting the very extensive storage capacity of the Potts network, quadratic in S [9,26]. Also the trajectories of the $S = 3$ homogeneous network are slower than in the random network, which does not have the memory attractors, but faster than the $S = 7$ ones. The effect of hybridization is then much stronger on the $S = 7$ units.

What happens when applying, after thermalization, an external input to some of the $S = 3$ units? Not much, Fig. 8(b) shows, if the simulated input is applied to half of them [following the procedure used for Fig. 7(c), with $\eta = 0.5$ and no clamp]. If $\eta = 1.0$, instead, i.e., the input is applied to the entire $S = 3$ subnetwork, then there is a major effect, particularly in producing immediate or very early divergence

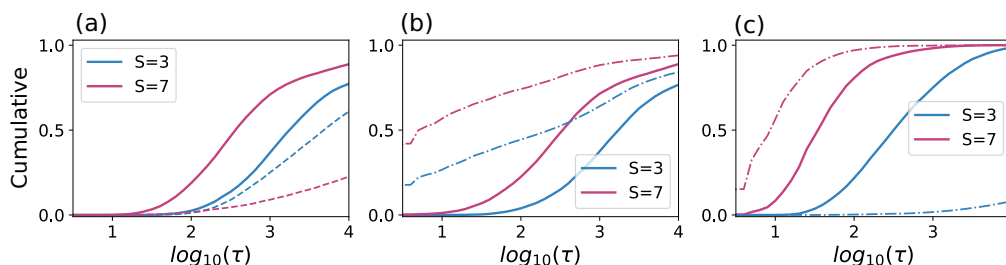


FIG. 8. Speed inversion occurs also in the associative memory model. (a) Cumulative distribution for τ (on a logarithmic scale) without external input. Dashed curves are for the homogeneous network. (b) The input-driven divergence times, i.e., when half of the $S = 3$ active units are perturbed ($\eta = 0.5$, solid curves) and all of the $S = 3$ active units are perturbed ($\eta = 1.0$, broken curves). (c) Asymmetric connections between the two subnetworks, obtained by removing or pruning 30% of them, results in only quantitative changes. The slowdown and also the speedup are dramatic, instead, when in addition, like in Fig. 7(c), the newly activated units are clamped by persistent external inputs (broken curves). For all panels, $T = 0.05$.

of many of the trajectories, but the speed inversion remains more or less unaltered (broken lines).

Finally, Fig. 8(c) shows that introducing moderate levels of asymmetry by diluting or cutting 30% of the connections *between* the two subnetworks does not have much of an effect either—unless one also clamps some of the units in the posterior network, in the manner already described; then, the posterior network slows down, almost to a standstill, which is intuitive, while surprisingly the anterior network speeds up further, as if unable to find any single satisfactory accommodation to the configuration imposed posteriorly.

V. DISCUSSION

Our study is premised on the hypothesis that some of the characteristics of cortical dynamics have their roots in the statistical physics of disordered systems [40]. Prior to attempting to validate the connection between two levels of analysis so distant from each other, we wanted to explore what the statistical properties might be, that might find—or not—their expression at the neural systems level. We have considered the reduction of Braitenberg’s model of cortical connectivity to a Potts network, and reviewed the thermodynamic analysis that predicts different types of transition from a paramagnetic to a glassy phase, as a function of the number S of local states. One should note that in this model the glassy character stems from the local attractor dynamics—the S states—whereas those very dynamics have been argued not to be too glassy, locally, if individual neurons are modeled realistically [41].

We then combine in a “hybrid” network two halves with “low” and “high” S units, inspired by the observed anatomical differences in the number of local synaptic connections—differences which, it should be remembered, may not lead, or only partially lead, to differences in the number of local attractor states. Surprisingly, in the “hybrid” network the low- S units are slowed down by the interaction, and the high- S ones are sped up, to the point of overtaking the former. This effect might be related to the different order of the phase transition to the glassy phase, but remarkably it is a reversal of the difference presented by homogeneous networks. Although one can construct seemingly intuitive explanations *a posteriori*, those did not enable us to *predict* it, in the least.

The speed inversion effect appears to survive largely unaltered the introduction of additional elements and details and, importantly, the replacement of the random network with an associative memory with connections structured by learning.

What are the implications for cortical processing? First, one should note that such implications should be taken with more than a grain of salt, if anything because the key concept of a single cortical axis is rather ill defined, at best. Perusing the many parameters of cortical circuitry that have been observed to vary across cortical areas, and the many more likely to be reported in the future, describing their variation as aligned to an axis, let alone whether it is the *same* axis across parameters, is a wishful simplification. The sensory-motor hierarchies conceptualized, e.g., by Fuster [42] have their final station in motor cortex *after* passing through the more anterior prefrontal cortices, while the termination layers of intracortical fibers, used to distinguish between feed-

forward and feedback projections, define a cortical hierarchy with the hippocampus at the top, the limbic cortices next to it just below, then the association cortices of both temporal and frontal lobes, going down all the way to primary sensory and motor cortices [43]. In terms of the number of largely local inputs to the basal dendrites of pyramidal cells, instead, Elston [44] gives estimates for areas V1, 7a, TE, and 12, in macaque monkey, that are roughly in the ratios 1:4:11:16, more or less along a posterior-to-anterior axis—but then measures in other areas do not necessarily align, for example, area 10 at the frontal pole is anterior to 12, but its pyramidal cells are estimated to have on average 17% fewer spines.

Our hybrid Potts network discards such complexity anyway to favor simplicity, and the speeding up of the large- S units that it reveals may have to be factored in, as an underlying phenomenon, in any complex scenario that envisages an imbalance between the effective numerosity of local attractor states across the cortical mantle. One scenario of this kind is the debate about the neural bases of consciousness, in which competing theories wrestle with the characterization of the differences between posterior and prefrontal cortices [45].

Interestingly, machine learning has pointed out the usefulness of combining “processing units” with memory properties at different timescales (*LSTM* units), e.g., to tackle syntax in language production and understanding. In particular, it has been predicted that long- and short-range units, which are taken to correspond to patches of cortex of perhaps 10^6 neurons, similar to our Potts units, should reside in different cortical regions [46]. Our findings should prove useful to research in this natural language processing framework, by at least contributing a warning that the properties of the units in a homogeneous network, or even in isolation, may differ, to the point of being the opposite, from those of the same units in a hybrid one.

A rather different linguistic domain in which the effective speed or slowness of glassy dynamics may be important is language evolution. There, it has long been hypothesized that the syntactic parameters that determine the internal structure of language and that evolve or even “mutate,” like units of a genetic code, on a scale of hundreds or thousands of years [47], may all be *binary*. Notably, many other features which are needed to describe natural languages and to implement them in artificial systems are obviously far from binary and appear to evolve, largely, on faster timescales. Our study suggests that in a network of parameters with effectively random interactions, those that emerge in evolution as more resistant to change, and therefore describe the most stable internal structure or set of *motifs* of a natural language, are precisely the binary ones, whether or not they possess a default value [48].

Yet other seemingly distant domains are those of protein folding and evolution, which have been approached with simplified Potts models [49,50]. The possible application of our results to these different fields is left for future work.

ACKNOWLEDGMENTS

This work was supported by PRIN Grant No. 20174TPEFJ “TRIPS” to Elisa Ciaramelli and A.T. We are also grateful to Francesco Rinaldi and Vezha Boboeva for their in-depth reading and criticism.

K.I.R. and A.T. developed the project as groundwork for another study to be reported elsewhere. K.I.R. went through the mathematical derivations and ran computer simulations. K.I.R. and A.T. jointly wrote the paper.

APPENDIX A: THE FREE ENERGY OF THE RANDOM POTTS GLASS MODEL

The free energy of the homogeneous model of Sec. III A is written, using the replica method, as

$$f = \lim_{n \rightarrow 0} \frac{1}{n} f_n,$$

$$\beta n f_n[\{q_{\gamma\delta}\}] = \frac{(\beta J)^2 \lambda^4}{2} \sum_{\gamma < \delta} q_{\gamma\delta}^2 + (\beta J)^2 \lambda^4 \sum_{\gamma=1}^n q_{\gamma\gamma}^2 - \ln \sum_{\sigma^1=0}^S \sum_{\sigma^2=0}^S \cdots \sum_{\sigma^n=0}^S \exp(K),$$

$$K \equiv (\beta J)^2 \lambda^4 \sum_{\gamma < \delta} q_{\gamma\delta} \sum_{k=1}^S V_\gamma^k V_\delta^k + (\beta J)^2 S \sum_{\gamma=1}^n q_{\gamma\gamma} (1 - \delta_{\sigma\gamma 0}) - \beta U \sum_{\gamma=1}^n (1 - \delta_{\sigma\gamma 0}), \quad (\text{A1})$$

where $q_{\gamma\delta}$ is the Edward-Anderson order parameter [30], $\beta = 1/T$ is the inverse temperature, and replica indices γ and δ run from 1 to n . The saddle-point equations of Eqs. (A1) are

$$q_{\gamma\delta} = \frac{\sum_{\sigma^1=0}^S \sum_{\sigma^2=0}^S \cdots \sum_{\sigma^n=0}^S [\sum_{k=1}^S V_\gamma^k V_\delta^k \exp(K)]}{\sum_{\sigma^1=0}^S \sum_{\sigma^2=0}^S \cdots \sum_{\sigma^n=0}^S \exp(K)}, \quad \gamma \neq \delta,$$

$$q_{\gamma\gamma} = \frac{S-1}{2S} \frac{\sum_{\sigma^1=0}^S \sum_{\sigma^2=0}^S \cdots \sum_{\sigma^n=0}^S [(1 - \delta_{\sigma\gamma 0}) \exp(K)]}{\sum_{\sigma^1=0}^S \sum_{\sigma^2=0}^S \cdots \sum_{\sigma^n=0}^S \exp(K)}. \quad (\text{A2})$$

The physical meaning of $q_{\gamma\delta}$ ($\gamma \neq \delta$) is the same as in the SK model [51] (see also Ref. [52]), while $2q_{\gamma\gamma}S/(S-1)$ is the fraction of active units in replica γ of the Potts network. Note that the free energy in Eq. (A1) does not depend on J_0 , the mean of the normal distribution from which the J_{ij}^{kl} 's are sampled. This is in contrast with the ES model [29], where low enough values of J_0 should be chosen to avoid ferromagnetic ordering at low temperatures [29,33]. Since the symmetry in our model is local—a sort of *gauge* invariance—there is no meaning to ferromagnetic alignment.

APPENDIX B: THE FREE ENERGY WITH REPLICAS SYMMETRY BREAKING

Following Landau [53], the free energy, Eq. (A1), can be expanded close to the critical temperature T_c , assuming $q_{\gamma\delta}$ ($\gamma < \delta$) to be small, to find

$$\beta n f_n \approx \frac{A}{2} \sum_{(\gamma\delta)} q_{\gamma\delta}^2 - \frac{B}{3} \sum_{(\gamma\delta)} q_{\gamma\delta}^3 - \frac{C}{3} \sum_{(\gamma\delta\lambda)} q_{\gamma\delta} q_{\delta\lambda} q_{\lambda\gamma} - \frac{D}{12} \sum_{(\gamma\delta)} q_{\gamma\delta}^4,$$

$$A = \frac{(\beta J)^2}{2} \frac{S^2}{S-1} [1 - (\beta J)^2 S^2 \psi^2],$$

$$B = \frac{(\beta J)^6}{4} \frac{S-2}{\sqrt{S-1}} S^2 \psi^2,$$

$$C = \frac{(\beta J)^6}{2} \frac{S^3 \psi^3}{\sqrt{S-1}},$$

$$D = (\beta J)^8 \left[\frac{3(3S-1)}{4(S-1)} S^4 \psi^4 - 3S^3 \psi^3 + \frac{S^2 - 3S + 3}{4(S-1)} S^2 \psi^2 \right]. \quad (\text{B1})$$

Here $(\gamma\delta\lambda)$ means that replica indices γ, δ, λ are all distinct in the summation. Following Ref. [32], we have retained only the quartic term that is relevant for RSB in Eqs. (B1). We have also assumed that the order parameter $q_{\gamma\gamma}$ does not depend on the replica index γ near T_c and thus have introduced a symbol $\psi \equiv 2q_{\gamma\gamma}/(S-1)$ to reduce the burden of heavy notation.

1. Properties at all temperatures

At temperatures well below T_c and when the transition is discontinuous, one should directly deal with the free energy, Eqs. (A1), in the full RSB formalism. Even for the SK model, solving Parisi's equations requires sophisticated numerical techniques (see Ref. [54]). However, Potts spins seem to have a distinguishing property from Ising spins, at least when we compare the ES model with the SK model: while any finite-step RSB solution is unstable in the SK model [31], the first-step RSB (1RSB) solution is locally stable in the ES model ($S > 2$) below T_c , down to a certain temperature, where another phase transition occurs [33,34]. So, one can study discontinuous transitions for $S > 4$, where the Landau expansion does not apply, by using a 1RSB formalism [55]. Here we use this method to study the discontinuous transition of our random Potts model, Eq. (2).

The Edward-Anderson order parameter is set as, within the 1RSB formalism,

$$q_{\gamma\delta} = \begin{cases} \tilde{q}, & \gamma = \delta \\ q_1, & \gamma \neq \delta, \lfloor \frac{\gamma}{m} \rfloor = \lfloor \frac{\delta}{m} \rfloor \\ q_0, & \gamma \neq \delta, \lfloor \frac{\gamma}{m} \rfloor \neq \lfloor \frac{\delta}{m} \rfloor, \end{cases} \quad (\text{B2})$$

where $\lfloor x \rfloor$ gives the smallest integer which is greater than or equal to x . Then the free energy reads

$$f[q_1, q_0, m] = \frac{\beta^2 J^2}{4} \lambda^4 [m(q_1^2 - q_0^2) - q_1^2] + \beta^2 J^2 \lambda^4 \tilde{q} - \frac{1}{m} \int \left(\prod_{l>0} D z_l \right) \ln \int \left(\prod_{k>0} D y_k \right) L^m, \quad (\text{B3})$$

where

$$L \equiv \sum_{\sigma=0}^S \exp \left\{ \left[\beta^2 J^2 S \left(\tilde{q} - \frac{q_1 - q_0}{2} \right) - \beta U \right] (1 - \delta_{\sigma 0}) + \beta J \lambda^2 \sum_{l>0} (\sqrt{q_0} z_l + \sqrt{q_1 - q_0} y_l) V_{\sigma}^l \right\} \quad (\text{B4})$$

and

$$D y \equiv \frac{d y}{\sqrt{2\pi}} \exp \left(-\frac{y^2}{2} \right). \quad (\text{B5})$$

Solving Eq. (B3) numerically is computationally hard, especially for large values of S . Thus, we restrict ourselves to a special case: the threshold U goes to $-\infty$ (the zero state then drops out of the equations). Inspired from the shape of Eq. (9), we seek solutions of the form

$$P(q) = m\delta(0) + (1 - m)\delta(q). \quad (\text{B6})$$

Then, the 1RSB free energy becomes

$$\beta f \approx \frac{(\beta J)^2 \lambda^4}{4} (m - 1) q^2 + \frac{(\beta J)^2 \lambda^4}{2} \frac{m + S - 1}{S} q - \frac{1}{m} \ln \int D \vec{y} \left[\sum_{l=1}^S \exp(\beta J \lambda^2 \sqrt{q} y_l) \right]^m, \quad (\text{B7})$$

where

$$D \vec{y} \equiv \prod_{k=1}^S \left[\frac{d y_k}{\sqrt{2\pi}} \exp \left(-\frac{y_k^2}{2} \right) \right].$$

We can numerically maximize Eq. (B7) by using the same numerical trick as in Ref. [55], up to $S = 20$. Critical temperatures obtained that way are reported in Fig. 3(b), while the order parameters are shown here in Fig. 9.

2. Extension to a hybrid network

In the case of a hybrid network, one obtains the free energy,

$$\beta n f_n \approx \frac{(\beta J)^2}{2} \sum_{\gamma<\delta} q_{\gamma\delta}^2 - \sum_{l=1}^L \eta_l \ln \text{Tr}^l \times \exp \left[(\beta J \lambda_l)^2 \sum_{\gamma<\delta} q_{\gamma\delta} (\delta_{\sigma\gamma\sigma\delta} - 1/S_l) \right], \quad (\text{B8})$$

where $q_{\gamma\delta}$ is the Edward-Anderson order parameter,

$$q_{\gamma\delta} = \frac{1}{N} \sum_{i=1}^N \lambda_i^2 \langle \delta_{\sigma_i^{\gamma} \sigma_i^{\delta}} - 1/S_i \rangle, \quad (\text{B9})$$

and

$$\text{Tr}^l \equiv \sum_{\sigma^1=1}^{S_1} \cdots \sum_{\sigma^l=1}^{S_l}. \quad (\text{B10})$$

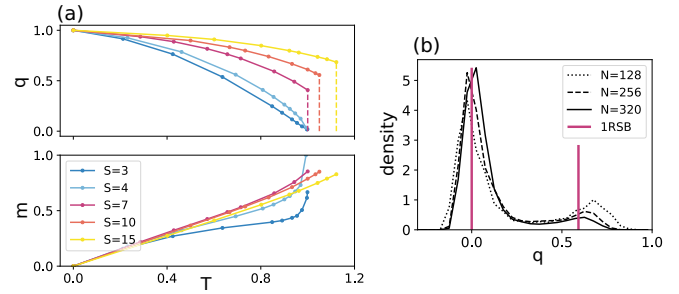


FIG. 9. Order parameters of a homogeneous Potts network without a zero state ($U \rightarrow -\infty$), predicted by 1RSB theory. (a) Solutions of the 1RSB free energy as a function of T . Note the discontinuous jumps in q at $T = T_c$ for $S > 4$. (b) Probability density, $P(q)$, obtained from Monte Carlo simulations, for $S = 7$ and $T \approx \frac{6}{7} T_c$. Red vertical lines indicate Dirac delta functions, estimated from (a). The peak at higher q seems to be lower with increasing values of N , but this is due to the insufficient relaxation time in our simulations. Since the relaxation time grows exponentially with N [38], we did not attempt to obtain the exact ground states.

As before, we expand Eq. (B8) around $q_{\gamma\delta} = 0$ and apply the Parisi algebra [56] to probe the nature of the equilibrium state. The corresponding free energy functional and the Parisi function that maximizes it have the same form as for the homogeneous network [see Eqs. (B1), (8), and (9)], after a redefinition of the coefficients A , B , C , and D , as follows:

$$\begin{aligned} A &= \frac{(\beta J)^2}{2} [1 - (\beta J)^2], \\ B &= \frac{(\beta J)^6}{4} \sum_{l=1}^L \eta_l \frac{S_l - 2}{\sqrt{S_l - 1}}, \\ C &= \frac{(\beta J)^6}{2} \sum_{l=1}^L \eta_l \frac{1}{\sqrt{S_l - 1}}, \\ D &= \frac{(\beta J)^8}{4} \sum_{l=1}^L \eta_l \frac{S_l^2 - 6S_l + 12}{S_l - 1}, \end{aligned} \quad (\text{B11})$$

leading to the conclusions reported in the main text.

APPENDIX C: THERMODYNAMICS FOR THE ASSOCIATIVE MEMORY NETWORK

The free energy is obtained by the replica trick (see Ref. [57] for the Hopfield model and Refs. [26,27] for the Potts model):

$$\begin{aligned} n f_n[\vec{m}, \mathbf{q}, \mathbf{r}] &= \frac{1}{2} \sum_{\gamma} (m_{\gamma})^2 + \frac{\alpha}{2\beta} \text{Tr} \ln[\mathbf{I} - \beta \tilde{\mathbf{a}} \mathbf{q}] \\ &+ \sum_{\gamma\delta} r_{\gamma\delta} q_{\gamma\delta} + \left[\frac{\alpha \tilde{a}}{2} + \frac{S U}{S - 1} \right] \\ &\times \sum_{\gamma} q_{\gamma\gamma} - \frac{1}{\beta} \langle \ln \text{Tr}_{\{\sigma\gamma\}} \exp[\beta L_{\sigma}^{\xi}] \rangle_{\xi}, \end{aligned} \quad (\text{C1})$$

where

$$L_\sigma^\xi \equiv \sum_\gamma m_\gamma \sum_{k>0} (\delta_{\xi k} - \tilde{a}) V_\gamma^k + \sum_{\gamma\delta} r_{\gamma\delta} \sum_{k>0} V_\gamma^k V_\delta^k \quad (C2)$$

and $\alpha \equiv p/N$ is taken to be $\alpha \neq 0$. The saddle-point equations read

$$\begin{aligned} m_\gamma &= \sum_{k>0} \langle (\delta_{\xi k} - \tilde{a}) \langle V_\gamma^k \rangle_{L_\sigma^\xi} \rangle_\xi, \\ q_{\gamma\delta} &= \left\langle \sum_{k>0} \langle V_\gamma^k V_\delta^k \rangle_{L_\sigma^\xi} \right\rangle_\xi, \\ r_{\gamma\delta} &= \frac{\alpha \tilde{a}}{2} [\mathbf{I} - \beta \tilde{a} \mathbf{q}]_{\gamma\delta}^{-1} - \delta_{\gamma\delta} \left[\frac{\alpha \tilde{a}}{2} + \frac{SU}{S-1} \right], \end{aligned} \quad (C3)$$

where

$$\langle X(\sigma, \xi) \rangle_{L_\sigma^\xi} \equiv \frac{\text{Tr}_\sigma [X(\sigma, \xi) \exp(\beta L_\sigma^\xi)]}{\text{Tr}_\sigma \exp(\beta L_\sigma^\xi)}. \quad (C4)$$

At high enough values of T and α , in fact, we expect retrieval solutions not to exist. So, we set $m_\gamma = 0$ and the terms including ξ and m_γ drop out of the equations. We can easily see that $q_{\gamma\delta}$ and $r_{\gamma\delta}$ are zero in the high-temperature limit, if $\gamma \neq \delta$. We expand the free energy with respect to these two variables around zero,

$$\begin{aligned} n\beta f \approx & \frac{n\alpha}{2} \ln(1 - \beta \tilde{a} \tilde{q}) + \beta \sum_{(\gamma\delta)} r_{\gamma\delta} q_{\gamma\delta} + n\beta \tilde{q} \left(\frac{\alpha \tilde{a}}{2} + \frac{SU}{S-1} + \tilde{r} \right) \\ & - \frac{\alpha \Lambda^2}{2} \left(\frac{1}{2} \sum_{(\gamma\delta)} q_{\gamma\delta}^2 + \frac{\Lambda}{3} \sum_{(\gamma\delta\lambda)} q_{\gamma\delta} q_{\delta\lambda} q_{\lambda\gamma} + \frac{\Lambda^2}{4} \sum_{(\gamma\delta\lambda\mu)} q_{\gamma\delta} q_{\delta\lambda} q_{\lambda\mu} q_{\mu\gamma} \right) \\ & - (S-1)\beta^2 \psi^2 \left\{ \sum_{(\gamma\delta)} r_{\gamma\delta}^2 + \frac{4\beta\psi}{3} \sum_{(\gamma\delta\lambda)} r_{\gamma\delta} r_{\delta\lambda} r_{\lambda\gamma} + \frac{2\beta(S-2)}{3S} \sum_{(\gamma\delta)} r_{\gamma\delta}^3 \right. \\ & \left. + \beta^2 \left[\psi^2(3S-1) - 4\psi \frac{S-1}{S} + \frac{S^2-3S+3}{4S^2} \right] \sum_{(\gamma\delta)} r_{\gamma\delta}^4 \right\}, \end{aligned} \quad (C5)$$

where

$$\Lambda \equiv \Lambda(T) = \frac{\beta \tilde{a}}{1 - \beta \tilde{a} \tilde{q}} = \frac{\tilde{a}}{T - \tilde{a} \tilde{q}}.$$

For the sake of simplicity, let us consider a RS ansatz. Then, the free energy reads, up to the third order in q and r ,

$$\begin{aligned} \beta f_{\text{RS}} \approx & \frac{\alpha}{2} \ln(1 - \beta \tilde{a} \tilde{q}) - \beta r q + \beta \tilde{q} \left(\frac{\alpha \tilde{a}}{2} + \frac{SU}{S-1} + \tilde{r} \right) \\ & + \frac{\alpha \Lambda^2}{4} q^2 \left[1 - \frac{4}{3} \Lambda q \right] + (S-1)\beta^2 \psi^2 r^2 \\ & \times \left[1 - \frac{8}{3} \beta \psi r + \frac{2(S-2)}{3S} \beta r \right]. \end{aligned} \quad (C6)$$

This free energy is maximized with respect to r and q , while \tilde{q} and \tilde{r} satisfy

$$\begin{aligned} \tilde{q} &= (S-1)\psi, \\ \tilde{r} &= \frac{\alpha \tilde{a}}{2} \left(\frac{1}{1 - \beta \tilde{a} \tilde{q}} - 1 \right) - \frac{S}{S-1} U, \\ \psi &= \frac{\exp(\beta \tilde{r} \frac{S-1}{S})}{1 + S \exp(\beta \tilde{r} \frac{S-1}{S})}. \end{aligned} \quad (C7)$$

In addition to the trivial (paramagnetic) solution of $q = 0$, we have

$$q = 2 \frac{\alpha \Lambda^2 \psi^2 (S-1) - 1}{\alpha \psi^2 \Lambda^3 (S-1) (4 + \alpha \Lambda \frac{4S\psi + 2 - S}{S})}. \quad (C8)$$

Numerically solving the above equations gives the transition temperature $T_c(U, \alpha)$ for the emergence of a glassy solution with small $q \neq 0$, as a function of U and α , provided that $\alpha \neq 0$ —what is reported in Fig. 10(b).

The limit of a finite number of patterns

When the tensorial weights encode only a finite number p of patterns, that is, $\alpha = p/N \rightarrow 0$ as $N \rightarrow +\infty$, we hypothesize that solutions corresponding to the retrieval of

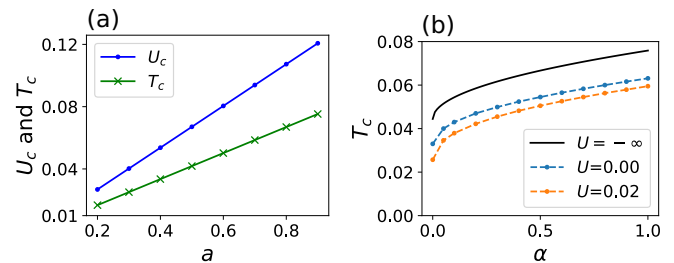


FIG. 10. High-temperature phase of associative memory for $S = 3$. (a) Maximum value of U (blue) above which the transition is no longer continuous, and the corresponding critical temperature (green) are plotted against sparsity of patterns for $\alpha \rightarrow 0$. (b) Critical temperature as a function of α for $a = 0.2$. Note that the data points for $\alpha = 0$ [in the panel (a), and the leftmost of the panel (b)] are computed separately from those for $\alpha \neq 0$, and that the sample value $U = 0.02$ used in the panel (b) is just below $U_c \approx 0.026$ given by solving the equations valid for $\alpha = 0$, in the panel (a).

one pattern, the so-called Mattis states, arise when lowering T at the critical value T_c which is the limit for $\alpha \rightarrow 0$ of the $T_c(U, \alpha)$ considered above. This is in fact the case for the Hopfield model [57]—but not necessarily for other network models (see Ref. [58]).

As $\alpha \rightarrow 0$, the q terms disappear from the free energy, Eq. (C1), and one can study Mattis solutions of Eqs. (C3), which satisfy

$$m = a \frac{\sum_{\sigma > 0} (\delta_{\sigma 1} - 1/S) \exp[\beta m (\delta_{\sigma 1} - 1/S) - \beta U]}{1 + \sum_{\sigma > 0} \exp[\beta m (\delta_{\sigma 1} - 1/S) - \beta U]}. \quad (\text{C9})$$

The critical temperature $T_c(U, 0)$ where $m \rightarrow 0$, for a given value of U , is determined by solving

$$T_c = \tilde{a}(S - 1) \frac{\exp(-U/T_c)}{1 + S \exp(-U/T_c)}. \quad (\text{C10})$$

The trivial solution of Eqs. (C3), $\vec{m} = 0$, is stable as long as the corresponding eigenvalue

$$\lambda = 1 - \frac{\tilde{a}(S - 1)}{T} \frac{\exp(-U/T)}{1 + S \exp(-U/T)} \quad (\text{C11})$$

remains positive. This is always the case for $T > T_c(U, 0)$. We can thus compute the maximum value of U , below which Mattis states arise.

We can see that if $U \rightarrow +\infty$, $T_c \rightarrow 0$ and the trivial solution $\vec{m} = 0$ is stable for all temperatures. In Fig. 10(a), we show values of U_c and the critical temperature at $U = U_c$. Figure 10(b) shows that $T_c(U, 0)$ is indeed very close to the limit of $T_c(U, \alpha \rightarrow 0)$.

TABLE I. Parameters of the network.

Symbol	Meaning	Default value
N	Number of Potts units	256
S	Number of states per unit	7 (3)
T	Temperature (noise level)	0.5
γ	Degree of asymmetry	0.2
η	Fraction of units with external inputs	0.5
p	Number of memory patterns	1024
t_0	Number of thermalization updates	1000
a	Mean activity	0.25

APPENDIX D: DETAILS ON THE COMPUTER SIMULATIONS

For models with a quiet state, the Edward-Anderson order parameter is computed as, instead of Eq. (20),

$$q_{\gamma\delta} = \frac{S}{S - 1} \frac{\sum_{i=1}^N (\delta_{\sigma_i^\gamma \sigma_i^\delta} - 1/S)(1 - \delta_{\sigma_i^\gamma 0})(1 - \delta_{\sigma_i^\delta 0})}{\sum_{i=1}^N (1 - \delta_{\sigma_i^\gamma 0})(1 - \delta_{\sigma_i^\delta 0})}. \quad (\text{D1})$$

The mean activity of the network is controlled by a time-dependent threshold

$$U(t) = U_0 + k \left[\frac{1}{N} \sum_i (1 - \delta_{\sigma_i 0}) - a \right]^3, \quad (\text{D2})$$

where a is the sparsity of patterns in the associative memory model and k is set as 1000. For the Potts glass model with a quiet state, we have used the same activity level a .

The external input to the posterior subnetwork is modeled by persistent external fields (after thermalization) to a fraction η of its units, which will maintain its states during dynamics (clamping in the main text). Specifically, we randomly select a fraction η of all active units in the $S = 3$ subnetwork. Among the selected units, a fraction a of them is flipped into a different active state, while the remaining fraction $1 - a$ of them is set into a quiet state. The same number of units among quiet units is activated to maintain the same level of activity.

If not specified explicitly, parameters are set as in Table I.

-
- [1] D. J. Amit, *Modeling Brain Function: The World of Attractor Neural Networks* (Cambridge University Press, Cambridge, UK, 1989).
- [2] G. A. Carpenter and S. Grossberg, The art of adaptive pattern recognition by a self-organizing neural network, *Computer* **21**, 77 (1988).
- [3] A. Treves and E. T. Rolls, Computational constraints suggest the need for two distinct input systems to the hippocampal CA3 network, *Hippocampus* **2**, 189 (1992).
- [4] V. Braitenberg and A. Schütz, *Anatomy of the Cortex: Statistics and Geometry* (Springer, Berlin, 1991).
- [5] P. L. Nunez, The brain wave equation: A model for the EEG, *Math. Biosci.* **21**, 279 (1974).
- [6] P. Valdés, J. Bosch, R. Grave, J. Hernandez, J. Riera, R. Pascual, and R. Biscay, Frequency domain models of the EEG, *Brain Topogr.* **4**, 309 (1992).
- [7] D. Daini, G. Ceccarelli, E. Cataldo, and V. Jirsa, Spherical-harmonics mode decomposition of neural field equations, *Phys. Rev. E* **101**, 012202 (2020).
- [8] V. Braitenberg, *Cortical architectonics: General and areal*, in *Architectonics of the Cerebral Cortex* (Raven Press, 1978), pp. 443–465.
- [9] I. Kanter, Potts-glass models of neural networks, *Phys. Rev. A* **37**, 2739 (1988).
- [10] A. Treves, Frontal latching networks: A possible neural basis for infinite recursion, *Cognit. Neuropsychol.* **22**, 276 (2005).
- [11] D. Spalla, I. M. Cornacchia, and A. Treves, Continuous attractors for dynamic memories, *eLife* **10**, e69499 (2021).
- [12] E. Russo and A. Treves, Cortical free-association dynamics: Distinct phases of a latching network, *Phys. Rev. E* **85**, 051920 (2012).

- [13] K. Il Ryom, V. Boboeva, O. Soldatkina, and A. Treves, Latching dynamics as a basis for short-term recall, *PLoS Comput. Biol.* **17**, e1008809 (2021).
- [14] G. N. Elston, R. Benavides-Piccione, and J. DeFelipe, The pyramidal cell in cognition: A comparative study in human and monkey, *J. Neurosci.* **21**, RC163 (2001).
- [15] E. K. Miller, C. A. Erickson, and R. Desimone, Neural mechanisms of visual working memory in prefrontal cortex of the macaque, *J. Neurosci.* **16**, 5154 (1996).
- [16] P. Rotshtein, R. N. A. Henson, A. Treves, J. Driver, and R. J. Dolan, Morphing Marilyn into Maggie dissociates physical and identity face representations in the brain, *Nat. Neurosci.* **8**, 107 (2005).
- [17] C. C. Hilgetag, A. Goulas, and J.-P. Changeux, A natural cortical axis connecting the outside and inside of the human brain, *Network Neurosci.* **6**, 950 (2022).
- [18] E. M. Meyers, D. J. Freedman, G. Kreiman, E. K. Miller, and T. Poggio, Dynamic population coding of category information in inferior temporal and prefrontal cortex, *J. Neurophysiol.* **100**, 1407 (2008).
- [19] A. R. Damasio and D. Tranel, Nouns and verbs are retrieved with differently distributed neural systems, *Proc. Natl. Acad. Sci. USA* **90**, 4957 (1993).
- [20] A. Daniele, L. Giustolisi, M. C. Silveri, C. Colosimo, and G. Gainotti, Evidence for a possible neuroanatomical basis for lexical processing of nouns and verbs, *Neuropsychologia* **32**, 1325 (1994).
- [21] L. K. Tyler, R. Russell, J. Fadili, and H. E. Moss, The neural representation of nouns and verbs: Pet studies, *Brain* **124**, 1619 (2001).
- [22] M. T. Ullman, Contributions of memory circuits to language: The declarative/procedural model, *Cognition* **92**, 231 (2004).
- [23] I. Tsuda, Toward an interpretation of dynamic neural activity in terms of chaotic dynamical systems, *Behav. Brain Sci.* **24**, 793 (2001).
- [24] V. Boboeva, R. Brasselet, and A. Treves, The capacity for correlated semantic memories in the cortex, *Entropy* **20**, 824 (2018).
- [25] K. I. Ryom, D. Stendardi, E. Ciaramelli, and A. Treves, Computational constraints on the associative recall of spatial scenes, *Hippocampus* **33**, 635 (2023).
- [26] E. Kropff and A. Treves, The storage capacity of Potts models for semantic memory retrieval, *J. Stat. Mech.* (2005) P08010.
- [27] M. Naim, V. Boboeva, C. Jun Kang, and A. Treves, Reducing a cortical network to a Potts model yields storage capacity estimates, *J. Stat. Mech.* (2018) 043304.
- [28] J. J. Hopfield, Neural networks and physical systems with emergent collective computational abilities, *Proc. Natl. Acad. Sci. USA* **79**, 2554 (1982).
- [29] D. Elderfield and D. Sherrington, The curious case of the Potts spin glass, *J. Phys. C: Solid State Phys.* **16**, L497 (1983).
- [30] S. F. Edwards and P. W. Anderson, Theory of spin glasses, *J. Phys. F* **5**, 965 (1975).
- [31] G. Parisi, A sequence of approximated solutions to the SK model for spin glasses, *J. Phys. A: Math. Gen.* **13**, L115 (1980).
- [32] G. Parisi, The order parameter for spin glasses: A function on the interval 0-1, *J. Phys. A: Math. Gen.* **13**, 1101 (1980).
- [33] D. J. Gross, I. Kanter, and H. Sompolinsky, Mean-Field Theory of the Potts Glass, *Phys. Rev. Lett.* **55**, 304 (1985).
- [34] V. Janiš and A. Klíř, Mean-field solution of the Potts glass near the transition temperature to the ordered phase, *Phys. Rev. B* **84**, 064446 (2011).
- [35] D. Bollé, R. Cools, P. Dupont, and J. Huyghebaert, Mean-field theory for the q -state Potts-glass neural network with biased patterns, *J. Phys. A: Math. Gen.* **26**, 549 (1993).
- [36] H. Sompolinsky and A. Zippelius, Dynamic Theory of the Spin-Glass Phase, *Phys. Rev. Lett.* **47**, 359 (1981).
- [37] M. Aguilera, M. Igarashi, and H. Shimazaki, Nonequilibrium thermodynamics of the asymmetric Sherrington-Kirkpatrick model, *Nat. Commun.* **14**, 3685 (2023).
- [38] A. P. Young, Direct Determination of the Probability Distribution for the Spin-Glass Order Parameter, *Phys. Rev. Lett.* **51**, 1206 (1983).
- [39] A. Treves and D. J. Amit, Metastable states in asymmetrically diluted Hopfield networks, *J. Phys. A: Math. Gen.* **21**, 3155 (1988).
- [40] M. Mézard, Spin glasses and optimization in complex systems, *Europhys. News* **53**, 15 (2022).
- [41] A. Treves, Are spin-glass effects relevant to understanding realistic auto-associative networks? *J. Phys. A: Math. Gen.* **24**, 2645 (1991).
- [42] J. Fuster, *The Prefrontal Cortex* (Academic Press, New York, 2015).
- [43] H. Barbas and N. Rempel-Clower, Cortical structure predicts the pattern of corticocortical connections, *Cereb. Cortex* **7**, 635 (1997).
- [44] G. N. Elston, Pyramidal cells of the frontal lobe: All the more spinous to think with, *J. Neurosci.* **20**, RC95 (2000).
- [45] M. Lenharo, Decades-long bet on consciousness ends—and it's philosopher 1, neuroscientist 0, *Nature (London)* **619**, 14 (2023).
- [46] Y. Lakretz, S. Dehaene, and J.-R. King, What limits our capacity to process nested long-range dependencies in sentence comprehension? *Entropy* **22**, 446 (2020).
- [47] G. Longobardi and C. Guardiano, Evidence for syntax as a signal of historical relatedness, *Lingua* **119**, 1679 (2009).
- [48] G. Longobardi and A. Treves, Grammatical parameters from a gene-like code to self-organizing attractors, [arXiv:2307.03152](https://arxiv.org/abs/2307.03152).
- [49] S. Cocco, R. Monasson, and M. Weigt, From principal component to direct coupling analysis of coevolution in proteins: Low-eigenvalue modes are needed for structure prediction, *PLoS Comput. Biol.* **9**, e1003176 (2013).
- [50] S. Cocco, C. Feinauer, M. Figliuzzi, R. Monasson, and M. Weigt, Inverse statistical physics of protein sequences: A key issues review, *Rep. Prog. Phys.* **81**, 032601 (2018).
- [51] D. Sherrington and S. Kirkpatrick, Solvable Model of a Spin-Glass, *Phys. Rev. Lett.* **35**, 1792 (1975).
- [52] G. Parisi, Infinite Number of Order Parameters for Spin-Glasses, *Phys. Rev. Lett.* **43**, 1754 (1979).
- [53] D. J. Amit, Renormalization of the Potts model, *J. Phys. A: Math. Gen.* **9**, 1441 (1976).
- [54] A. Crisanti and T. Rizzo, Analysis of the ∞ -replica symmetry breaking solution of the Sherrington-Kirkpatrick model, *Phys. Rev. E* **65**, 046137 (2002).

- [55] E. De Santis, G. Parisi, and F. Ritort, On the static and dynamical transition in the mean-field Potts glass, *J. Phys. A: Math. Gen.* **28**, 3025 (1995).
- [56] G. Parisi, Magnetic properties of spin glasses in a new mean field theory, *J. Phys. A: Math. Gen.* **13**, 1887 (1980).
- [57] D. J. Amit, H. Gutfreund, and H. Sompolinsky, Statistical mechanics of neural networks near saturation, *Ann. Phys.* **173**, 30 (1987).
- [58] D. Bollé, P. Dupont, and J. Huyghebaert, Thermodynamic properties of the q -state Potts-glass neural network, *Phys. Rev. A* **45**, 4194 (1992).